Dead time corrections for Bonner sphere measurements of secondary neutrons at a proton therapy facility

Dommert, M.; Reginatto, M.; Zbořil, M.; Lutz, B.;

Originally published:

March 2021

Journal of Instrumentation 16(2021), P03038

DOI: https://doi.org/10.1088/1748-0221/16/03/P03038

Prepared for submission to JINST

Dead time corrections for Bonner sphere measurements of secondary neutrons at a proton therapy facility

Martin Dommert,[a] **Marcel Reginatto,**[a] **Miroslav Zbořil,**[a] **Benjamin Lutz**[b,1]

[a] *Physikalisch-Technische Bundesanstalt, Braunschweig, Germany*

[b] *Helmholtz-Zentrum Dresden - Rossendorf, Institute of Radiation Physics, Dresden, Germany*

E-mail: b.lutz@hzdr.de

Abstract: Radiation therapy with proton beams allows the deposition of high doses to the tumour while minimising dose to the surrounding tissue. During such treatment the patient is also exposed to secondary radiation which produces an out-of-field dose that affects healthy tissue. The largest contribution to this out-of-field dose comes from neutron radiation; therefore, it is of interest to fully characterise the neutron field in the therapy room with measurements. This is usually done with Bonner sphere spectrometers using active detectors, typically ^{3}He-filled proportional counters, as central thermal neutron sensors. Under the experimental conditions encountered in proton therapy facilities, a proper analysis of the measurements is impossible unless dead time corrections are implemented. In this paper, we present a method using a paralysable dead time model for carrying out such corrections for Bonner sphere measurements with ^{3}He-filled proportional counters and apply it to data taken at the University Proton Therapy Dresden (UPTD) facility in double scattering mode. The neutron events were recorded with time stamps and, based on this time-resolved data, the measured neutron rate distribution was sampled. Since the neutron flux is proportional to the proton flux, the integral neutron flux is directly related to the proton dose. Hence, we were able to estimate the detector dead time from the measured rate distributions recorded for a set of measurements with different proton dose rates. Experimental measurements with different intensities of the proton field show that the corrections are in agreement within 0.5% for measured signal rates smaller than 15×10^3 counts per second and do not exceed 1% at 25×10^3 counts per second.

Keywords: Neutron detectors, Instrumentation for hadron therapy, Data processing methods, Radiation monitoring

[1]Corresponding author.

Contents

1 Introduction

The use of proton beams in radiation therapy has the advantage, when compared for example to photon therapy, that the tumour can be exposed to high doses while minimising the dose to surrounding tissue [1]. The treatment typically involves protons with energies in the range of 70 to 250 MeV. During treatment with proton beams the patient is also exposed to secondary radiation, in the form of neutrons, photons and charged particles, which produces an out-of-field dose which affects healthy tissue. The determination of the additional dose from secondary radiation is of importance in order to assess the risk of secondary cancers [2, 3]. Neutron radiation provides the largest contribution to this out-of-field dose [4] and it can be of concern in the case of paediatric treatments and the treatment of pregnant patients.

Estimates of the out-of-field dose require accurate information about the quality and extent of the neutron radiation component for specific facilities, as a function of beam delivery and for particular patient configurations. Therefore, it is important to carry out measurements to characterise the neutron field in the therapy room under conditions that reproduce those that are used in clinical treatments. Such measurements are not straightforward. One critical issue is that proton therapy facilities operate with time varying beam settings. As a result, the secondary neutron field exhibits a complex time variation which makes the accurate correction of detector dead time effects difficult when measuring at high absolute rates, which are precisely the ones that are required for clinical treatment. A proper analysis of neutron spectrometric measurements with active detectors is impossible unless dead time corrections are implemented.

We have carried out Bonner sphere measurements at the facility of the University Proton Therapy Dresden (UPTD) using the extended-range Bonner sphere spectrometer of the Physikalisch-Technische Bundesanstalt (PTB). For the analysis of these measurements, we have developed a dead time model that is applicable to the system for the given measurement conditions. The validity of the approach has been tested with a series of measurements carried out with different beam currents. The focus of this paper is on this dead time analysis.

The paper is structured as follows. In the next two sections, we describe the spectrometer used for the measurements and show examples of the distortion of the pulse-height spectra that occurs due to dead time and pile-up effects. We then discuss dead time models and present the method developed for the dead time correction. We end with a discussion and conclusion. An appendix describes the time structure of the neutron flux in double scattering mode.

2 The extended-range Bonner sphere spectrometer NEMUS

Spectral measurements of secondary neutrons in proton therapy facilities present a number of challenges. At a minimum, the spectrometer must be capable of covering a wide energy range that extends from thermal energies to a few hundred MeV and the resolution of the spectrometer must be sufficient to bring out the important features of the spectrum. These two basic requirements can be handled by extended-range Bonner sphere spectrometers, which have proven to be well suited for measurements in high-energy fields [5]. However, the measurements are not straightforward because proton therapy facilities are operated with time varying beam settings. The beam current is typically both pulsed as well as varying in current, and the beam energy is a function of time. Consequently, the secondary neutron field exhibits a complex time variation. This poses a challenge for the accurate correction of detector dead time effects when measuring with Bonner sphere spectrometers at high rates.

An extended-range Bonner sphere spectrometer consists of a set of moderating spheres of different diameters and a thermal neutron sensor that is placed at the centre of each sphere. A typical set has spheres made of polyethylene plus a few modified spheres with metal shells embedded in polyethylene spheres to increase the response to high-energy neutrons (i.e., at neutron energies above ~50 MeV). In addition, it is usual practice to measure also with the thermal neutron sensor without a moderating sphere (i.e., the bare detector). Any combination of sphere and thermal neutron sensor is usually called a "sphere" and this terminology has also been extended to the bare detector. Each sphere plus thermal sensor combination has a different energy response to neutrons, which is what enables a determination of the spectrum from measurements with different spheres using unfolding methods.

PTB operates an extended-range Bonner sphere spectrometer known as NEMUS [6]. It consists of 10 standard polyethylene spheres with diameters 3, 3.5, 4, 4.5, 5, 6, 7, 8, 10 and 12 inches.[1] The set also contains a bare detector, a Cd-covered detector, and four modified spheres with lead or copper shells. The central thermal sensors are spherical ^{3}He-filled proportional counters of type SP9 He3/152/Kr [7] manufactured by Centronic. For this particular set of measurements, we used proportional counters with partial ^{3}He-pressures of ~200 kPa and ~20 kPa. The proportional

[1]The convention of labeling each sphere by its diameter in inches has developed over the years and will be applied in this work (1 inch = 2.54 cm).

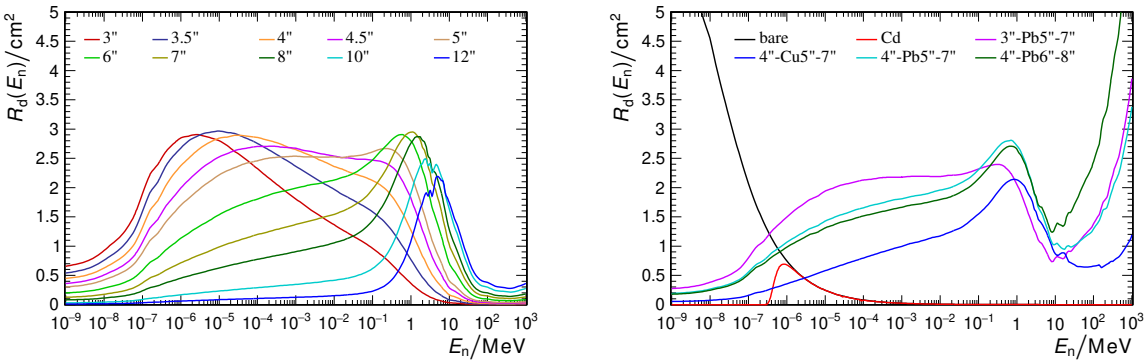

Figure 1. Response matrix of the NEMUS extended-range Bonner sphere spectrometer [6]. The response of the 10 polyethylene spheres are shown on the left side. The right side shows the response of the bare detector, the Cd-covered detector, and the four modified spheres with a lead or copper shell inserted. The names of the modified spheres indicate the outer radii of the polyethylene core, the metal shell, and the surrounding polyethylene shell.

counters with lower pressure are less sensitive to neutrons and thus less affected by dead time, therefore, these are used at locations where the neutron intensity is higher. Figure 1 shows the response matrix of the NEMUS spectrometer with the ~200 kPa proportional counter. The readout system of the NEMUS spectrometer consists of a shaping amplifier and a digitisation stage, as well as a data acquisition system. The block diagram shown in figure 2 displays the main components used for measurements with the NEMUS system. The shaping of the detector signal is performed by an AIOSAP-02 (All In One Spectrometry Analogue Processor Version 2 [8]), a PTB in-house development. The AIOSAP was specifically developed for the use with ^{3}He-filled proportional counters and combines a charge sensitive pre-amplifier, a shaping amplifier, and the detector high voltage power supply. The shaping time of the detector signal is approximately 2 μs. The digitisation stage is a peak-sensing analogue-to-digital converter (ADC) of type Dual ADC Model 7072, ADC/SVA [9] manufactured by FAST Comtec GmbH. For data acquisition a multi-channel analyser of type MPA4 Multiparameter Data Acquisition System (8 channel) [10] manufactured by FAST Comtec GmbH is used. The MPA4 Multiparameter System is designed as an ultra fast list mode system and allows for measurements of eight ADC input channels in parallel. In addition to simple acquisition of the ADC pulse-height spectra, the system is able to save time resolved data points, if operated in *list mode*; i.e., the pulse-height with a corresponding time stamp is recorded for each detected event. The event time is recorded in units of 6.4 ns.

3 Pulse-height spectra of spherical ^{3}He-filled proportional counters

The data collected with a spherical ^{3}He-filled proportional counter, used as a thermal detector in a Bonner sphere, is in the form of a pulse height spectrum. The detection of neutrons takes place by means of the reaction ^{3}He(n,p)T (with a reaction Q value of +764 keV and a thermal neutron cross section of 5321 barn). The counts in this spectrum are used to determine the number of neutron induced events.

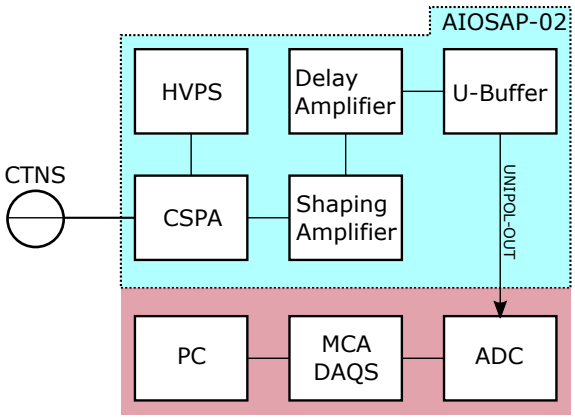

Figure 2. Block diagram of electronics used for measurements with the NEMUS Bonner sphere spectrometer and a ^{3}He-filled central thermal neutron sensor (CTNS). Necessary components such as the detector high-voltage power supply (HVPS), charge sensitive pre-amplifier (CSPA), and further components used for the analogue processing of the detector signal are contained in a single AIOSAP-02 unit [8]. The output of the AIOSAP-02 is connected to a peak-sensing analogue-to-digital converter (ADC) which is read by a multi channel analyser data acquisition system (MCA DAQS).

The left plot of figure 3 shows a pulse height spectrum from a measurement made under controlled conditions; i.e., good statistics, no noise or gamma-induced events in the lower channels, and a rate that is low enough to exclude pile-up events and lead to negligible dead time. The full-energy peak on the right part of the spectrum corresponds to the reaction energy of 764 keV. The events in the lower channels are due to the partial escape of the proton and/or triton from the active volume of the counting gas (wall effect). The lower limit of the neutron induced events, at about channel 100, corresponds to the full escape of the proton (573 keV) implying the full energy dissipation of the triton (191 keV) in the gas. In the case of measurements made under controlled conditions as in the left plot of figure 3, the neutron signal can be determined in a straightforward manner by setting appropriate thresholds summing the number of counts in the region-of-interest.

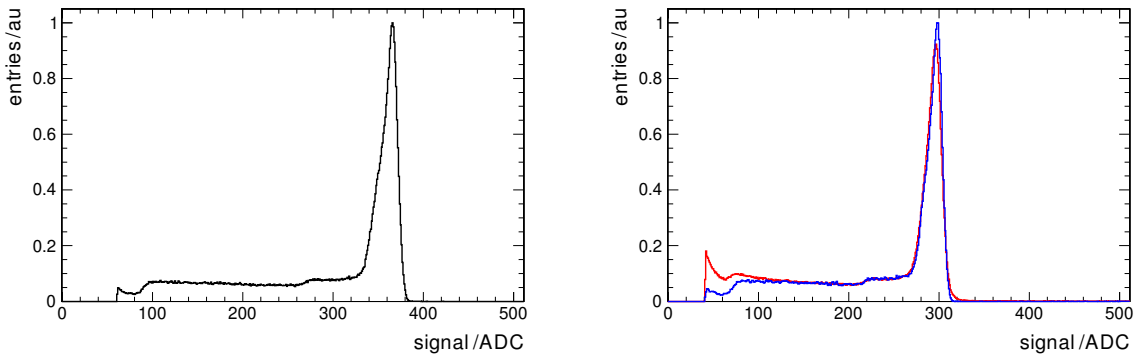

Figure 3. Left: pulse-height spectrum (PHS) of a ^{3}He-filled proportional counter obtained from a measurement made under controlled conditions. Right: measured PHS with gamma induced events in the low channels (red) together with a fitted reference spectrum (blue).

Under more difficult measurement conditions, a number of corrections must be included in the analysis. There are two main types of corrections, to account for non-neutron signals in the lower channels of the pulse-height spectrum which are often induced by photons, and to account for dead time and distortions of the spectrum caused by pile-up. Counts due to non-neutron events will typically contribute to the dead time.

The right plot of figure 3 shows a measured pulse height spectrum that is distorted by gamma induced events in the lower channels (red) together with a reference spectrum measured under controlled conditions with the same proportional counter (blue) that has been fitted to the region that is not affected by the gamma induced events. The correction is straightforward whenever the gamma induced events do not extend past ~50% of the maximum energy over which the neutron deposits a signal (i.e., the full energy peak). After carrying out the fitting procedure, the reference spectrum is used to determine the total number of neutron induced events.

A different type of corrections is required for the data in figure 4 which show distortions that are due to pile-up effects and indicative of substantial amounts of dead time. The plots are for measurements made for different primary proton beam intensities and counters with gas pressures of ~200 kPa and ~20 kPa (the ~200 kPa counters are more efficient than the ~20 kPa counters due to the difference in gas pressure and, therefore, more susceptible to pile-up). The pile-up leads to significant shape changes of the pulse height spectrum for the 200 kPa pressure counters, shown on the left, while the 20 kPa pressure counters, shown on the right, are far less affected at the same beam current.

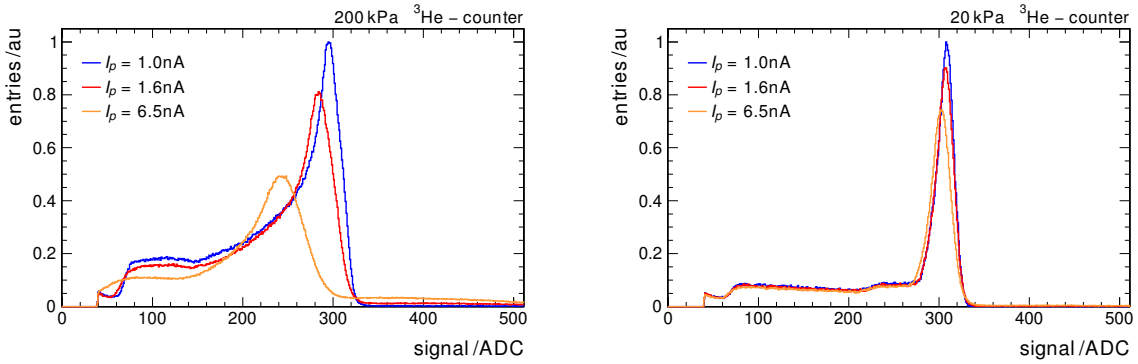

Figure 4. Pulse-height spectra obtained from measurements with varying primary proton beam intensity; i.e., I_p = 1.0 nA (blue), I_p = 1.6 nA (red) and I_p = 6.5 nA (yellow), with various types of distortion due to pile-up effects for counters with gas pressures of ~200 kPa (left) and ~20 kPa (right).

The changes of shape in the more distorted spectra of figure 4 are a clear indication of saturation effects in the system. Such effects cannot be easily corrected (if at all). Thus, it is important to limit measurements to count rates that cause only small distortions of the pulse height spectra, which can then be corrected for pile-up and dead time. As an example, if you consider the plots on the left side of figure 4, it turns out that reliable dead time corrections are possible for the cases of beam currents of 1 nA and 1.6 nA but not for the case of a beam current of 6.5 nA. It is always important to carry out a visual inspection of the spectra before attempting to carry out dead time corrections.

4 Dead time models

Detector dead time is defined as the minimum time interval between two consecutive events that is needed for both events to be counted by a detector. Due to dead time effects, measured counting rates will be lower than the actual counting rates; however, the real counting rate can be recovered if the dead time of the detector can be determined and the measurements corrected.

It is useful to consider two different models of dead time effects [11], known as paralysable and non-paralysable. In the first case, the time in which the system does not record a signal is extended whenever another signal arrives while the system is busy. In the second case, the system is always capable of recording the next signal after a time interval that is fixed. The two situations lead to different equations relating the real signal rate f_r and the rate measured by the system f_m:

$$f_\mathrm{m}^\mathrm{p} = f_\mathrm{r}\, e^{-f_\mathrm{r}\tau}, \tag{4.1}$$

$$f_\mathrm{m}^\mathrm{n} = \frac{f_\mathrm{r}}{f_\mathrm{r}\tau + 1}, \tag{4.2}$$

where τ is the dead time of the system. Equation (4.1) describes paralysable systems while equation (4.2) is valid for non-paralysable systems. Figure 5 shows measured signal rate versus real signal rate for paralysable and non-paralysable systems. The literature on dead time models is extensive and there are a number of criteria for choosing between different models [11, 12] but a full discussion of this issue lies outside of the scope of this paper.

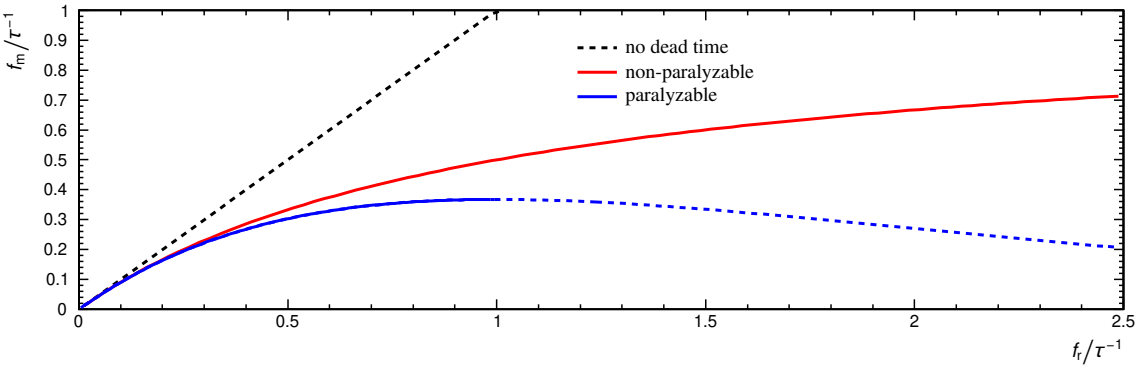

Figure 5. Measured signal rate versus real signal rate for paralysable and non-paralysable readout systems.

While the non-paralysable dead time model is a monotonically increasing function and therefore always invertible, the paralysable model has a maximum measurable rate and the function is not generally invertible: The relation between signal rate and measured rate is only unique for signal rates smaller than $1/\tau$. In this case, the maximal measurable rate is given by $f_\mathrm{max} = 1/(e\tau) \approx 0.37/\tau$.

Most systems have dead times which are not truly paralysable or non-paralysable. This can lead to a complex dead time behaviour which might not be easily correctable. However, in the case in which one domain dominates the dead time behaviour, a correction with one of the two described models can lead to reasonably good results. This is the case for the measurements carried out at the proton therapy facility with the NEMUS Bonner sphere spectrometer, which can be corrected using a paralysable model, as we now discuss.

The readout system consists of a shaping amplifier and a digitisation stage as described in section 2. The amplifier turns the input signal into a pulse with an amplitude proportional to the input charge and a pulse form defined by the integrated shaping. The shaped signal is then converted to a digital value by a peak sensing analogue-to-digital converter (ADC). An ADC readout cycle is triggered when the signal exceeds a certain amplitude threshold. By the operational principles of the ADC, a consecutive readout cycle can only be triggered when the conversion and data transfer times have passed and the signal has fallen below the trigger threshold. The ADC has a fixed conversion time of 500 ns and a fixed data transfer time of 100 ns after the signal peak has been reached [9]. Depending on the exact threshold setting, the shaped signal of a single pulse falls below the threshold after roughly 4 times the shaping time of approximately 2 μs.

Figure 6 shows the pulse shape of the signal after the amplifier, recorded with an oscilloscope. Two consecutive signals start to overlap when the time difference is too short, as is visible for the first two pulses. In this case, the ADC will not distinguish such nearby pulses as the signal does not fall below the threshold between pulses. This is the classical case of a paralysable dead time. As the conversion and data transfer time are much shorter than the signal duration, they always pass before the analogue signal has settled and do not contribute to the dead time. Consequently, the overall system dead time follows a paralysable dead time model.

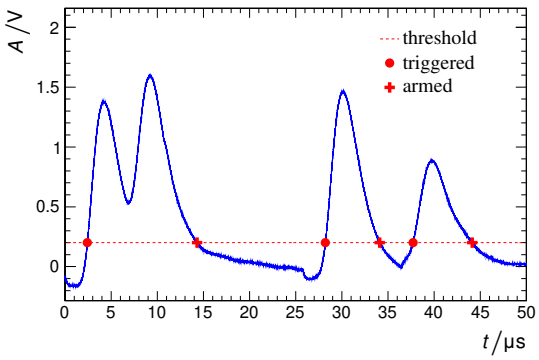

Figure 6. Pulse shape at the amplifier output. The blue line shows the amplitude A of the AIOSAP output versus time t. The red dashed line indicates the trigger threshold. Points where the ADC triggers and rearms are marked with red circles and crosses, respectively.

5 Dead time correction

In double scattering mode, the interplay of the different time variable components of the proton therapy system generates a complex variation of the beam current in time and the irradiation pattern (a description of the time structure of the neutron flux in double scattering is presented in the appendix). Furthermore, the system uses different range modulator tracks and beam current modulations for different range settings. Combined with the different settings for the modulation, this means that the proton therapy system can generate several thousand different time patterns. Therefore, a method that can estimate the dead time from the recorded data itself seems the only feasible approach for the analysis of the measurements considered here.

5.1 Correction method

To estimate the dead time from the data, we take into consideration that the ADC used in the readout systems has a count-rate capability of more than 1×10^6 counts per second and the data processing unit can record list-mode data with time stamps in units of 6.4 ns. This provides sufficient time resolution to sample the measured signal rate several times during a single rotation of the range modulator wheel. The samples can be used to estimate the distribution of the measured signal rate. As there is no synchronisation between data acquisition and wheel rotation and to achieve a constant uncertainty for the individual rate samples, the measured signal rate is calculated after a fixed number of recorded events (every 100 triggers) rather than for fixed time intervals. Figure 7 is an example of the measured signal rate for a ^{3}He-filled proportional counter inside a modified sphere for irradiation using double scattering mode.

Under the assumption that the measured signal rate is sampled faster than it changes, it is possible to apply the dead time correction to these individual sampling points. The real rate is calculated for each sampling point using a numeric inversion of equation (4.1), assuming a paralysable dead time model. Figure 8 shows the distribution of measured signal rate f_m and calculated real rate f_r. The peak at $3 \times 10^3\,\mathrm{s}^{-1}$ is an artefact and occurs when one sample is composed from events both before and after the beam pause during the range modulator wheel period. These entries are ignored in the calculations as they do not fulfil the requirement of sampling the rate faster than it changes.

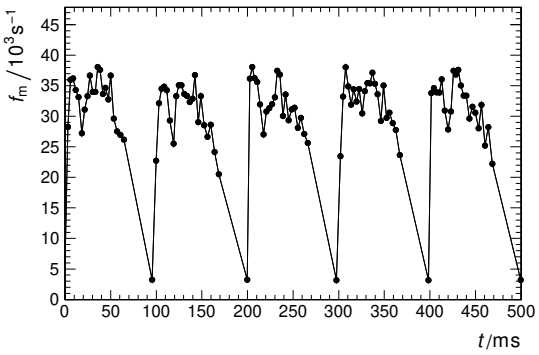

Figure 7. Measured signal rate f_m versus time t for a spherical ^{3}He-filled proportional counter inside a moderator sphere of lead and polyethylene. The signal rate is computed every 100 triggers.

We define the overall dead time correction factor c as the ratio of the measured number of signals N_m to the real number of signals N_r. It can be computed from the means of the measured signal rate f_m and the calculated real rate f_r:

$$c = \frac{N_\mathrm{r}}{N_\mathrm{m}} = \frac{< f_\mathrm{r} >}{< f_\mathrm{m} >} = \frac{\sum_i f_{i,\mathrm{r}}}{\sum_i f_{i,\mathrm{m}}} \tag{5.1}$$

5.2 Determination of the detector dead time

In order to derive the calculated real rate f_r from equation (4.1) and compute the dead time correction factor c from equation (5.1), the dead time τ of the detection system needs to be known. The value of the dead time τ depends on the shaping time and the chosen trigger threshold. Both properties

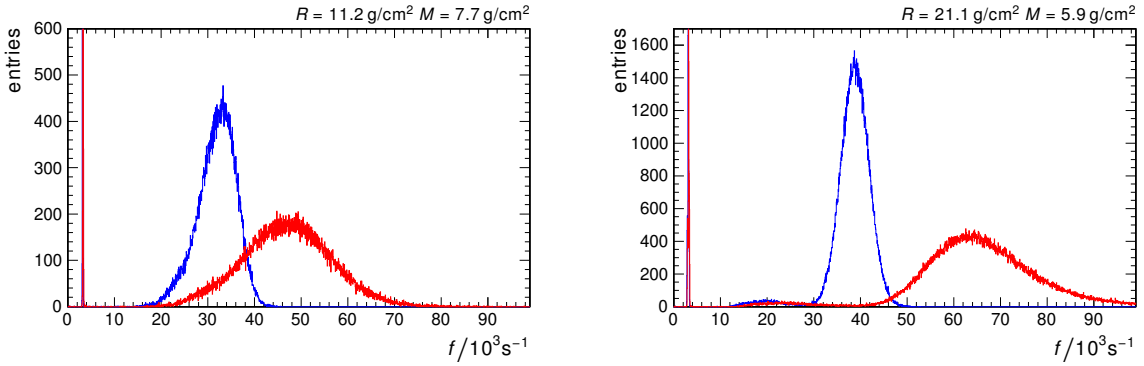

Figure 8. Histograms of measured and corrected rate over a long irradiation period for different settings for range R and modulation M (see the appendix for a discussion of the range R and the modulation M). The measured signal rates f_{m} are drawn in blue. The red histogram shows calculated real rates f_{r} assuming a paralysable dead time model with an optimised value for τ.

can vary for different readout channels. Consequently, τ has to be determined for each readout channel individually.

The neutron flux at proton therapy facilities is directly proportional to the proton flux, therefore, the integral neutron flux is directly related to the proton dose. The proton therapy system is designed to accurately deliver a prescribed dose to the patient. The reproducibility of the delivered proton dose is better than 0.5% independent of the selected dose rate [13]. Hence, the calculated real rate f_{r} of a detection system is directly related to the applied proton dose rate and the real number of signals N_{r} is related to the applied proton dose. This allows us to determine the dead time τ with the help of a dose rate scan where we change the primary proton current. We carried out three sets of dose rate scans for different proton range settings (see the appendix for a discussion of the range R and the modulation M). Each scan consisted of four different dose rate settings. For the different dose rate settings, we calculated the corrected number of neutron signals N_{r} assuming different values of τ based on the procedure introduced in the previous paragraph.

The left plot of figure 9 gives an example of one such dose rate scan and how the residual of dead time corrected number of signals varies assuming different dead time values. When the correct τ is chosen, the calculated number of neutrons N_{r} has to become independent of the dose rate and the slope of the linear fit to the residual values will equal zero. The right side of figure 9 displays the variation of the slope of the linear fit versus τ for the three recorded range settings. The optimal dead time value, used to calculate the dead time correction factor c for each individual readout channel, is determined as the mean of the three crossing points where the slope becomes zero.

The dead time value τ of the individual channels is approximated from dose rate scans for the three different range settings. The success of the dead time correction can be tested by calculating the residual variation between the measurements with different dose rates. Figure 10 summarises the result for all readout channels. The remaining fluctuations are below 0.5% for measured signal rates smaller than $15 \times 10^3\ \mathrm{s}^{-1}$ and do not exceed 1% for the maximally tested measured rate of approximately $25 \times 10^3\ \mathrm{s}^{-1}$

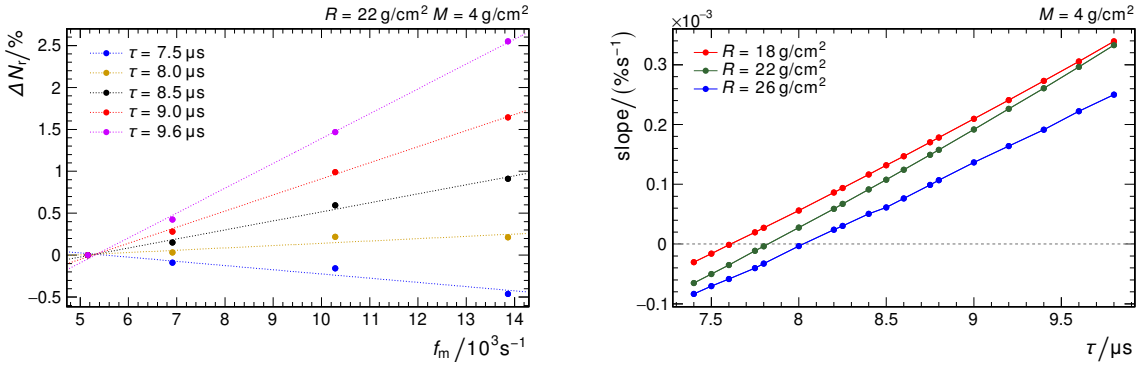

Figure 9. Left: Difference of the dead time corrected number of signals ΔN_r relative to the measurement with the lowest signal rate for one readout channel. The dotted lines show the linear fit for a specific value of τ. Right: Slope of the linear fit versus τ for three different proton range settings.

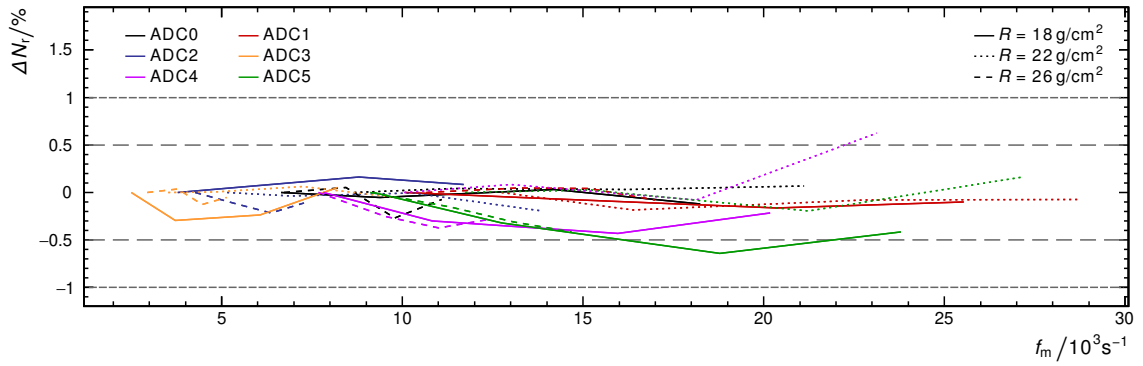

Figure 10. Difference of the dead time corrected number of signals relative to the measurement with the lowest signal rate. The line colour distinguishes the different readout channels. The three different proton range settings are differentiated by the line style.

6 Discussion

The method for dead time correction presented here is not restricted to proton therapy facilities. It is designed to work with all systems that have a long enough pulse duration that the rate can be sampled multiple times during one pulse. The choice to sample the rate every fixed number of events is practical as it creates samples with the same relative error and is easy to calculate. By discarding the samples that contain the beam pause, the bias from mixing very different rates in one sample is kept to a minimum. An alternative would be to sample with fixed time intervals. But, a good choice of the interval length would require an a priori knowledge of the rates as a minimum number of events per time slot should be achieved to get numerically stable results.

A clear limitation of the method is the requirement of long enough pulses. For repetitive signals, this might be overcome by sampling synchronised to the pulse start and collect statistics over several repetitions. Of course, this would require some synchronisation between beam delivery and data acquisition or a precise way to identify the pulse start in the recorded data. However, the signal patterns generated at a proton therapy facility operating in double scattering mode are well

suited for the suggested method. The applicability to other operation modes like pencil beam scanning has to be studied.

The suggested in situ determination of τ depends on an accurate knowledge of the applied amount of primary beam. This is readily available at therapeutic facilities, which are designed to reproduce an exact dose. At accelerators without such a precise beam control, an independent measurement of the applied amount of primary beam can be used to scale the measured counts.

7 Conclusion

The measurement of neutron fields at proton therapy facilities is technically challenging. One particular issue is the determination of the dead time for a measurement in a neutron field which is both pulsed and varying in intensity. This work describes a method to correct the dead time for complex rate distributions in case time-stamped data is available. Additionally, how the time constant τ can be determined in situ with the help of a rate scan is explained. The method was applied to measurements conducted at the University Proton Therapy Dresden operating in double scattering mode. After the correction, residual variations of the reconstructed number of events below 0.5% for measurement rates smaller than 15×10^3 counts per second (cps) and below 1% for rates up to 25×10^3 cps are achieved.

Appendix: Time structure of the neutron flux in double scattering mode

A spread-out Bragg peak (SOBP) is typically described by its range R and its modulation M. Different conventions are in use for these quantities. Here, the definition used for the IBA system is adopted. The range R is defined as the distance between the entrance point of the beam and the point in depth where the dose falls to 90% of the plateau level. Similarly, the modulation M is defined as the distance between the point where the dose level reaches 90% of the plateau dose and the point where it falls below 90% of the plateau dose.

Double scattering uses a rotating wheel with steps of variable thickness to modulate the beam energy and consequently vary the penetration depth (range) of the protons in the target. The height and width of the steps are designed such that a spread-out Bragg peak is generated when the wheel rotates at constant speed. The design also permits varying the length of the SOBP plateau (modulation) by stopping the beam before the wheel has completed a full rotation. Finally, the beam current is modulated with the rotation of the range modulator wheel (RMW) to compensate for production imperfections. This results in three different components for the time structure of the neutron flux.

The most prominent feature is the switching of the proton beam to adjust the modulation. Figure 7 shows the rate in a ^{3}He-filled proportional counter inside a moderator sphere versus time. The 10 Hz rotation of the wheel is clearly visible.

The varying proton energy leads to a second time component. The RMW always starts with an absorber that blocks the proton beam. The absorber is followed by modulator steps of increasing thickness. While the absorber is blocking the beam, neutrons are only generated in the RMW and upstream of it. This moves the neutron generation away from the target volume and reduces the neutron flux at the target location. Directly after the absorber, the neutron flux increases to its

peak as the protons reach the aperture of the scattering system with the highest energy. With the increasing size of the steps, the protons loose more energy at the range modulator wheel and the number of neutrons generated in the RMW increases while the neutron component generated by protons absorbed in the aperture reduces. This results in a net reduction of the rate at the target location.

The modulation of the beam current directly translates into a variation of the neutron flux and overlays the time variations that comes from the rotation of the wheel.

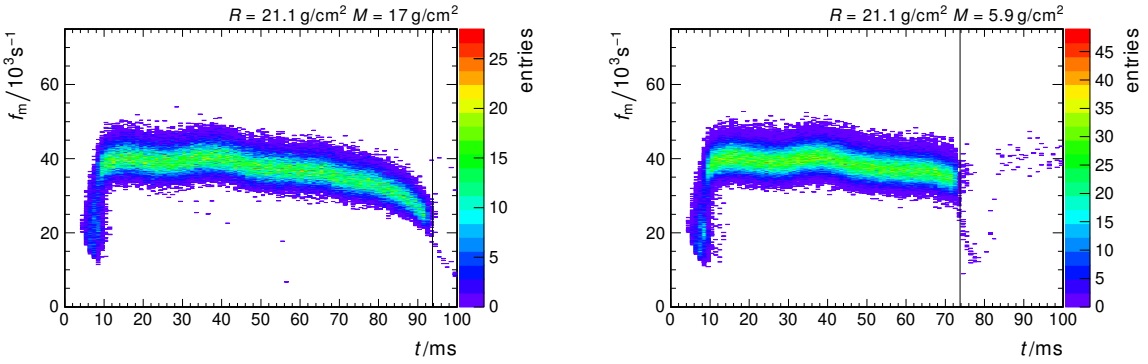

Figure 11. Measurements of the trigger rate of a ^{3}He-filled proportional counter in a moderator sphere for a proton range $R = 21.1$ g/cm^2 and modulation of $R = 17$ g/cm^2 (left) and $R = 5.9$ g/cm^2 (right). The trigger rate is plotted against the time after the range modulator wheel zero-crossing. The black line indicates the time when the proton beam is switched off.

Another aspect of the variation of the neutron flux with time can be seen in figure 11. The plot on the left shows the instantaneous rate in a ^{3}He-filled proportional counter versus the time calculated from the leading edge of the pulsed beam. The black line indicates the time when the proton beam is stopped to adjust the modulation. The plot on the right shows the same quantity with the same proton beam range setting but with decreased modulation. The shortening of the neutron pulse is clearly visible.

Figure 12 compares the mean rate measured by the ^{3}He-filled proportional counter with the beam current setting used to modulate the proton beam intensity. The low rate before the 10 ms point is due to the absorber block at the beginning of the range modulator. The variations in the neutron flux between 10 ms and 50 ms are mainly due to the variation of the beam current. At later times, the decrease of the neutron flux due to the reduction in proton range is dominant.

Acknowledgments

The authors would like to thank the University Proton Therapy Dresden for allowing access to their facility. Especially, we would like to thank Julia Thiele and her team for their hospitality. Special thanks go to Wolfgang Enghardt, Stefan Menkel, Julia Hytry, and Daniela Kunath for allowing us to record data during their quality assurance measurements. We also thank Ion Beam Applications (IBA Inc., Louvain la Neuve, Belgium) for providing us with detailed information about the working principles of their therapy system. Especially, we would like to thank Ryan Haneke-Swanson of the local IBA team for answering our many questions. Finally, we would like to thank Katja Römer,

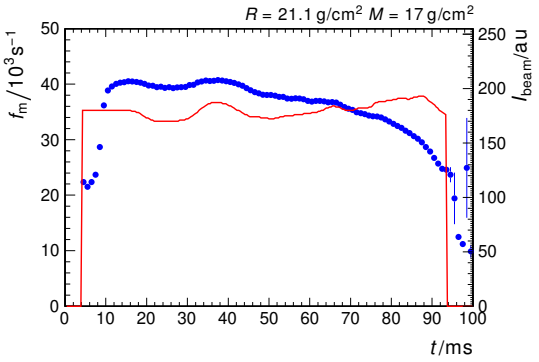

Figure 12. Mean measured neutron rate f_m (blue points) and primary proton beam current setting (red line) versus time within one range modulator wheel rotation.

Stephan Helmbrecht, Laura Dorn, André Lücke, and Thorsten Klages for their help in preparing and executing the Bonner sphere measurements.

References

[1] W. D. Newhauser and R. Zhang, *The physics of proton therapy*, *Phys. Med. Biol.* **60** (2015) R155.

[2] X. G. Xu, B. Bednarz and H. Paganetti, *A review of dosimetry studies on external-beam radiation treatment with respect to second cancer induction*, *Phys. Med. Biol.* **53** (2008) R193.

[3] W. D. Newhauser and M. Durante, *Assessing the risk of second malignancies after modern radiotherapy*, *Nat. Rev. Cancer* **11** (2011) 438.

[4] U. Schneider and R. Hälg, *The impact of neutrons in clinical proton therapy*, *Front. Oncol.* **5** (2015) 235.

[5] D. J. Thomas and A. V. Alevra, *Bonner sphere spectrometers – a critical review*, *Nucl. Instr. Meth. Phys. Res. A* **476** (2002) 12.

[6] B. Wiegel and A. Alevra, *NEMUS – the PTB neutron multisphere spectrometer: Bonner spheres and more*, *Nucl. Instr. Meth. Phys. Res. A* **476** (2002) 36 .

[7] Centronic LTD., *3He Proportional Counters General Data*, 4, 2005.

[8] A. V. Alevra, *All-In-One Spectrometry Analogue Processor AIOSAP-02, Manual*. Physikalisch-Technische Bundesanstalt, Braunschweig, 2008.

[9] FAST Comtec GmbH, Gruenwalder Weg 28A, 82041 Oberhaching, Germany, *Model 7072 Dual ADC - Data Sheet*, 2006.

[10] FAST Comtec GmbH, Gruenwalder Weg 28A, 82041 Oberhaching, Germany, *Model MPA4, 8 ch acquisition system with 6 ns time tagging*, 2011.

[11] V. Bécares and J. Blázquez, *Detector dead time determination and optimal counting rate for a detector near a spallation source or a subcritical multiplying system*, *Sci. Technol. Nucl. Install.* **2012** (2012) .

[12] S. Usman and A. Patil, *Radiation detector deadtime and pile up: A review of the status of science*, *Nucl. Eng. Technol.* **50** (2018) 1006 .

366 [13] C. Bäumer, B. Ackermann, M. Hillbrand, F.-J. Kaiser, B. Koska, H. Latzel et al., *Dosimetry*
367 *intercomparison of four proton therapy institutions in germany employing spot scanning*, *Z. Med.*
368 *Phys.* **27** (2017) 80 .